Materials Research Proceedings 28 (2023) 1977-1986 https://doi.org/10.21741/9781644902479-213

Microstructure analysis of hybrid aluminum parts from recycled EN AW-6082 and EN AW-7075 chips

URSINUS Jonathan[1,a *], KOCH Alexander[2,b], BRUNOTTE Kai[1,c], WALTHER Frank[2,d] and BEHRENS Bernd-Arno[1,e]

[1]Institute of Metal Forming and Machines (IFUM), Leibniz University Hannover, An der Universität 2, 30823 Garbsen, Germany

[2]Chair of Materials Test Engineering (WPT), TU Dortmund University, Baroper Str. 303, 44227 Dortmund, Germany

[a]ursinus@ifum.uni-hannover.de, [b]alexander3.koch@tu-dortmund.de, [c]brunotte@ifum.uni-hannover.de, [d]frank.walther@tu-dortmund.de, [e]behrens@ifum.uni-hannover.de

Keywords: Aluminum, Recycling, Chips, FAST, Extrusion, Hybrid Materials

Abstract. In order to promote aluminum scrap recycling and reduce remelting losses, solid-state recycling processes are subject to increasing academic attention. These processes range from severe plastic deformation (SPD) to diffusion-based processes like field-assisted sintering (FAST). In this study, a FAST-based recycling route consisting of precompaction, FAST, and impact extrusion of dry machined EN AW-6082 and EN AW-7075 aluminum chips was used to create multi-material parts from different aluminum alloys. To examine the effect on the resulting part quality, two different hybrid material layouts were created during cold compaction of the chips. The subsequent sintering process took place in a field-assisted sintering (FAST) machine at 400°C and 500°C for a duration of 5 min under a pressure of 85 MPa, allowing for the analysis of inter-chip diffusion. These sintered blanks were then cold-formed by impact extrusion. Metallographic and computed tomography analyses as well as hardness measurements were performed for property evaluation before and after heat-treatment.

Introduction

Aluminum alloys are widely used for products in all industrial sectors and numerous applications. In line with global economic growth, the global production of primary aluminum increased by 20 % from 49 megatons in 2012 to 59 megatons in 2016 [1]. In 2019, this production increased to 66 megatons globally [2]. Combined with 33 megatons of recycled secondary aluminum, the global annual aluminum industry processes 100 megatons, with a strictly increasing tendency. Considering the high energy requirements for the production of primary aluminum of roughly 13 MWh/t [3,4], the use of aluminum scrap for the production of secondary aluminum offers great potential for energy savings, as it requires only 5 % (0.7 MWh/t) of the primary process' energy demands [5]. Consequently, the fraction of secondary aluminum in global production is increasing [6], however with significant regional differences in scrap return rates [7].

As with most metals, the production processes mainly include casting, forming and machining. Aluminum products are either cast directly after the metallurgical production of the alloy or it is processed into semi-finished products, e.g. bars or sheets. These are then later formed or machined into the desired product. Most processing steps involve material losses, due to flash formation, burn-off, chip production and other reasons. Generally, primary scrap (e.g. from casting) can be directly recycled. However, contaminations and the high specific surface of chips and fine flash lead to oxidation and metal losses between 5 and 20 wt.% during conventional melt-metallurgical recycling [8]. Therefore, the development of solid-state recycling (SSR) techniques promises

advantages in material yield and energy consumption and may help to reduce material losses in a circular economy.

The origin of these SSR techniques dates back to 1945 when *Stern* received a patent on the recycling of aluminum scrap by hot extrusion [9]. Later, further investigation took place, while most research is younger than 20 years. *Gronostajski et al.* studied the extrusion of aluminum chips after ball milling and sintering [10] and the direct extrusion of the milled chips without sintering [11]. In both cases, nearly complete densification was achieved with tensile strengths of over 90 % of the base material reference [10,12]. The hot extrusion process was further studied by other researchers, focusing on bond formation [13], secondary extrusion [14], resulting material properties [15] and mathematical modelling [16]. These investigations share the general idea of applying pressure and temperature to the material during deformation and are part of a group of processes designated as severe plastic deformation (SPD) processes. The aim is to break up or disrupt the oxide layers covering the chips by applying pressure and deformation and thereby enable welding of the chip surfaces [17,18]. Other examples for SPD processes are equal channel angular pressure (ECAP) extrusion [19] or cyclic extrusion compression (CEC) [20]. With SPD processes, part geometry and deformation are determined by the process itself, with restricted process windows and therefore limited opportunity to consider part requirements.

An alternative approach involves the sintering of aluminum chips and a consolidation due to diffusion processes. While conventional die pressing and sintering requires milling of the chips into powder, pressure assisted sintering processes allow the direct processing of the chips after precompaction. Different authors were able to process aluminum chips by spark plasma sintering (SPS). *Paraskevas et al.* produced fully densified specimens from AA6061 and AA6082 chips by sintering at a temperature of 490°C and 200 MPa of axial pressure [21]. *Koch et al.* investigated the same alloy EN AW-6082 processed at different process parameters of 400°C and 40 MPa by field-assisted sintering technology (FAST). The sintered specimens were cold extruded and heat-treated (T6) to surpass the mechanical properties of the heat-treated reference [22]. A comparable pulsed electric current sintering (PECS) process was investigated on a smaller scale by *Cislo et al.*, using a Gleeble 3800 and a sintering temperature of about 450°C with a pressure of 64 MPa. The results showed an inhomogeneous microstructure and defective areas together with bonded parts [23]. While there are differences in the machinery used as well as in the application of the electrical current, the afore mentioned processes SPS, FAST and PECS share the same basic concept of directly heated pressure assisted sintering and are summarized using the term FAST [24]. They are in contrast to conventional hot pressing with indirect heating, which *Fogagnolo et al.* used for the recycling of AA6061 chips. These were sintered at a temperature of 500 °C and a pressure up to 700 MPa for 50 min. Nevertheless, the resulting microstructure required the authors to add hot extrusion as an additional consolidation process [25].

In summary, a variety of processes is proposed for SSR of aluminum chips. Especially FAST processes allow the consolidation of precompacted chips without major billet deformation. In this study, this aspect allows the production of hybrid specimens consisting of different aluminum alloys by recycling. This possibility is an inherent advantage compared to melt-metallurgical recycling and may help to improve part performance or to reduce the overall demand for high quality secondary alloys by a load-adapted component design. With forming operations, the sintered hybrid layout is deformed and adjusted to part requirements. At first, however, the general concept of layout creation and deformation is characterized and evaluated in the presented study. Furthermore, effects of material layout and sintering temperature on the resulting part geometry, defects and microstructure are investigated.

Experimental Setup

For the investigation, aluminum chips of the alloys EN AW-6082 and EN AW-7075 were used. The chips were produced by milling without the use of lubricant to eliminate the need for cleaning and its influence. The resulting chips' dimensions were measured manually and are given in Table 1 as mean values with standard deviation.

Table 1. Chip dimensions and apparent density.

Alloy	Length in mm	Width in mm	Height in mm	App. density in g/cm³
EN AW-6082	9.95 ± 1.80	1.01 ± 0.20	0.37 ± 0.05	0.25
EN AW-7075	6.42 ± 2.00	0.93 ± 0.07	0.18 ± 0.07	0.145

The chips were precompacted into briquettes using a manual hydraulic press with a pressure of 170 MPa. The precompacting step allowed different hybrid alloy layer designs:

(S) An axial layering consisting of three stacked briquettes with 30 g of chips each, 90 g in total. One briquette of EN AW-6082 was stacked between two briquettes of EN AW-7075.

(R) A radial layering created with the help of a specialized hollow punch tool. The inner core with a diameter of 15 mm consists of EN AW-7075 chips. For the outer material, EN AW-6082 chips were used.

All briquettes had an outer diameter of 35 mm. Fig. 1 shows a schematic of the cold compaction setup as well as the resulting hybrid layouts.

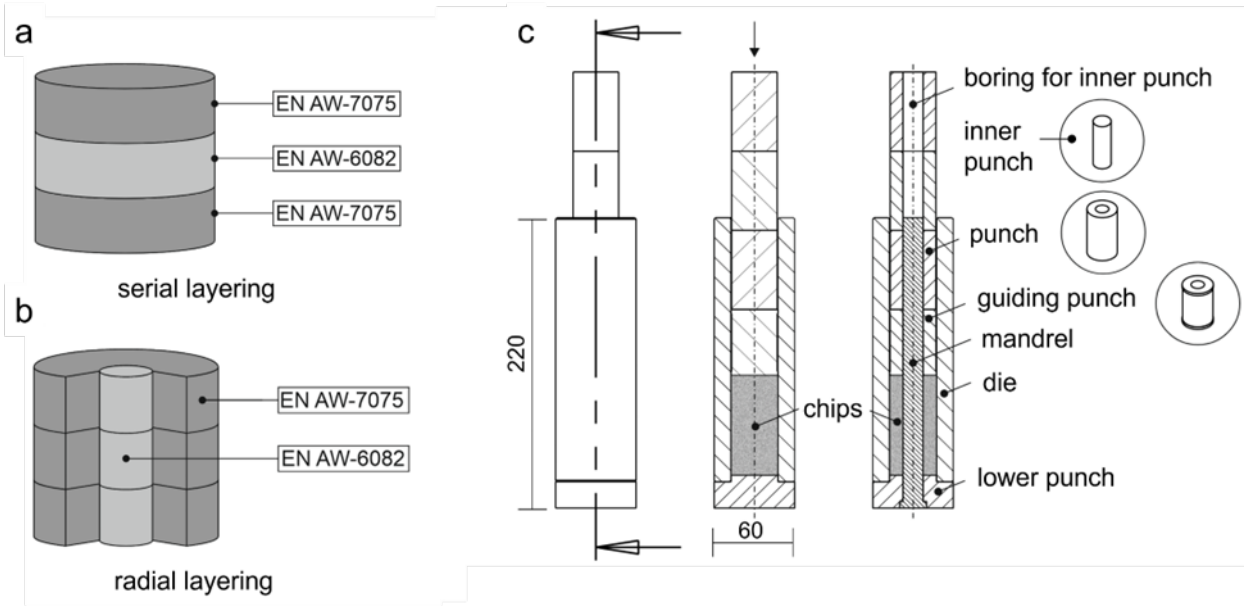

Fig. 1. Layout of the hybrid aluminum specimens, (a) axial layering strategy, (b) radial layering strategy and the used compaction tool (c).

After cold compaction, the three stacked briquettes were sintered using a Dr Fritsch DSP 507 FAST machine. The machine uses electrical current (DC) to directly heat the chip material by Joule heating. The temperature was measured by three thermocouples within the sintering die, with the highest value (generally TC 2) used for process power control. The tool setup with its components is depicted in Fig. 2.

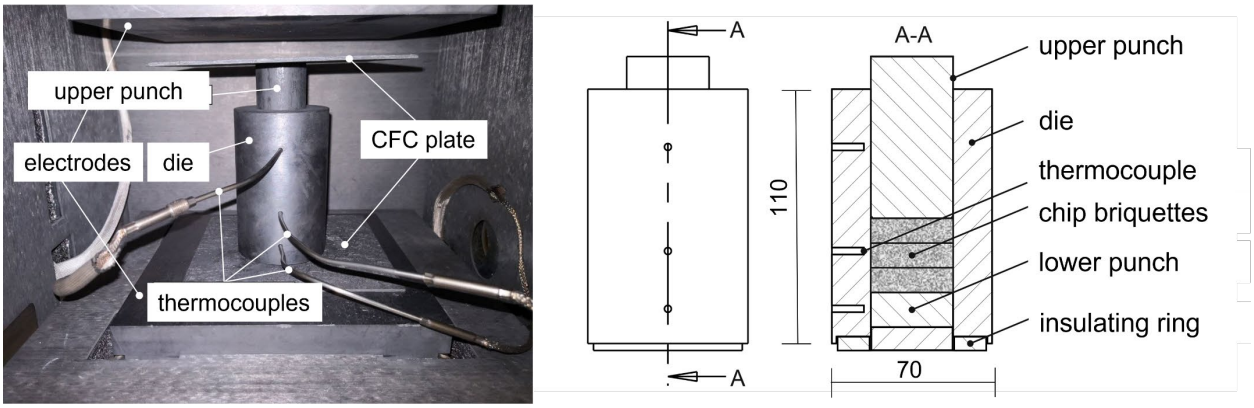

Fig. 2. Experimental setup of the field-assisted sintering process (left) and schematic representation of the sintering tool (right).

The hybrid layouts S and R were both sintered at two different temperatures of 400°C and 500°C for 5 mins resulting in 4 variants SL, SH, RL and RH. The sintering parameters given in Table 2 were based on previous experiments [22] and resulted all in above 99 % rel. density.

Table 2. Process variants.

Variant	Layout	Sintering temperature (°C)	Sintering time (s)	Sintering pressure (MPa)
SL	Serial	400	300	85
SH	Serial	500	300	85
RL	Radial	400	300	85
RH	Radial	500	300	85

After sintering, the specimens were air cooled and then analyzed using a Nikon XT H 160 computed tomography (CT) scanner. The scans were carried out using a current of 100 µA and an acceleration voltage of 150 kV resulting in a power of 15 W. By using a distance of 15 mm from the radiation source, a resolution of 40 µm could be achieved. The volume reconstructions were calculated with the help of Nikon CT Agent and analyzed with Volume Graphics VGStudioMax 2.2 software.

After performing the CT scans the specimens were formed using cold impact extrusion. Before extrusion the specimens were heated to 110°C and lubricated with LUBRODAL 24 W in a 1:2 solution with water. The resulting lubricant layer was dried for 24 h. The forming operation was carried out on a Weingarten PSR 160 screw press at room temperature. The diameter of the cylindrical specimens was reduced from 37 mm (including insertion tolerances for sintering and extrusion) to 16 mm, resulting in a mean plastic strain of $\varphi = 1.6$. The die shoulder angle was $2\alpha = 60°$ and the resulting extruded length was between 62 mm and 66 mm.

Subsequently, the specimens were scanned again by computed tomography. Furthermore, longitudinal sections were cut and investigated metallographically. Hardness measurements (HV 0.01) were performed within 5 mm of the interface in the centre of the shaft using a Shimadzu HMV-G automatic hardness testing device with a Vickers indenter and a force of 98.07 mN. EDX-line scans at the hybrid interface were performed on the SL and SH variants using Octane Elect Pro EDX detector by AMETEK Inc. in a Mira 3 SEM by Tescan. The cut specimens were then heat treated using a solution annealing temperature of 480°C. Water quenching cooled them rapidly to room temperature before cold aging. Finally, hardness measurements and metallographic examinations were repeated.

Results

The intermittent CT scans allowed the observation of the material distribution before and after cold extrusion. Combined with the metallographic analysis of the extruded specimens their deformation behavior and microstructural characteristic were investigated. The different alloy compositions cause transmissivity differences which allow the different materials to be distinguished. This results in EN AW-7075 material appearing brighter than EN AW-6082.

Before extrusion, the serial layouts SL and SH show a slight curvature of the axial interfaces in the CT images in Fig. 3. This is caused by friction forces acting on the outer diameter of the briquette stacks during sintering. As only the top punch moves in relation to the sintering die, this distortion, which is typical for one-sided compaction of powders, occurs.

After extrusion, the images show an elongation of the center of EN AW-6082 material into the surrounding EN AW-7075 material. This results in one half of the shaft being radially layered, however with a conical geometry of the interface. Consequently, the bonding surface between the two alloys was enlarged. The extruded SL specimen shows cracks at this interface near the extrusion shoulder, while for the SH-specimen no cracks could be observed.

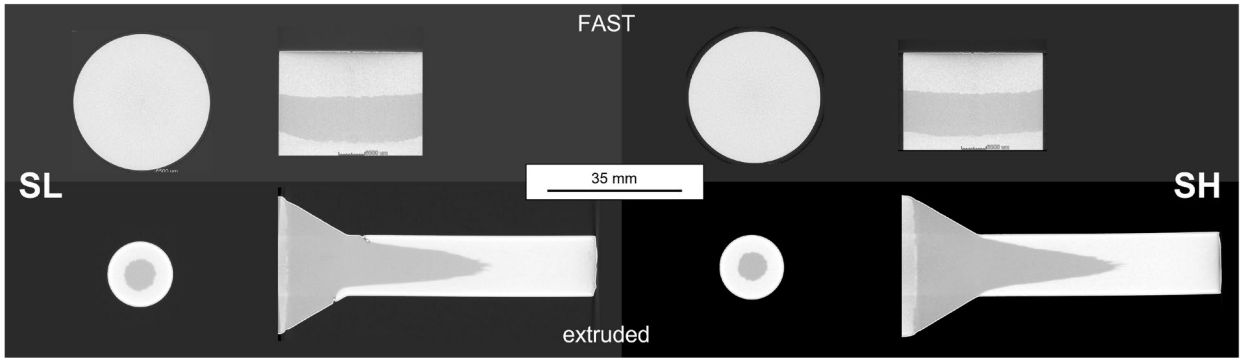

Fig. 3. CT imaging of the sintered (top) and extruded (bottom) serial specimens sintered at 400°C (left) and 500°C (right).

The radial layouts' material distribution before extrusion shows very limited deviation from the ideal concept, as can be seen in Fig. 4. There is no significant distortion of the interface during sintering and both alloys are still in coaxial arrangement. The extruded specimens exhibit a conical expansion of the softer EN AW-6082 material near the tip of the shaft, followed by a long section of uniform cross-section and material proportions. Both, the RL and RH specimens show cracks at the briquette interface at the tip of the extruded specimen. These are of reduced severity for the RH variant, which was sintered at higher temperature.

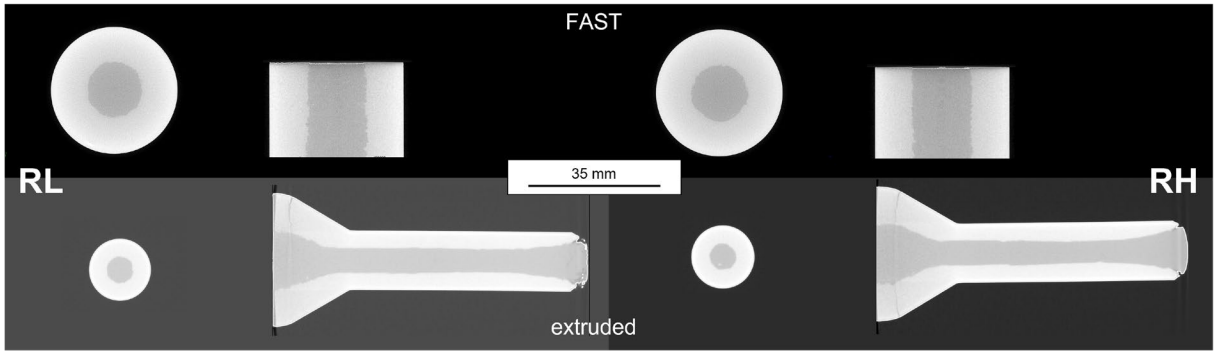

Fig. 4. CT imaging of the sintered (top) and extruded (bottom) radial specimens sintered at 400°C (left) and 500°C (right).

During the FAST process, changes in the microstructure occurred depending on the sintering temperature. After sintering at 400°C, the SL and RL variants showed a densified structure with some defects and the chip boundaries clearly visible as dark lines (see Fig. 5). The original sheared grain orientation is still prevalent within the individual chips of both alloys. By increasing the sintering temperature to 500°C for the SH and RH variant, the number of visible defects was significantly reduced and the former chip boundaries appear thinner. Additionally, grain growth and recrystallization can be observed for the EN AW-6082 material. At locations of thin or with missing chip boundary layer, grain recrystallization occurred across the interface, resulting in the visual disbanding of the dark oxide lines. In case of the EN AW-7075 material, the sheared microstructure of the chips remained visible within all four variants. After sintering at 500°C, the interface between both alloys shows signs of diffusion processes, indicated by a separation of the chip boundary oxide layer and the line of color change after etching.
Fig. 6a shows the results of the EDX line scans across the interface. The Al signal increases abruptly when crossing the interface of the SL specimen from EN AW-7075 to EN AW-6082, as the alloying element concentration drops. However, the graph for the SH specimen shows a gradual increase, confirming the metallographic observation of a pronounced diffusion zone. The microhardness results for the sintered conditions given in Fig. 6b show low values of 80 to 100 HV 0.01 for EN AW-7075 and 40 to 60 HV 0.01 for EN AW-6082 material. The values increase with increasing sintering temperature for both alloys.

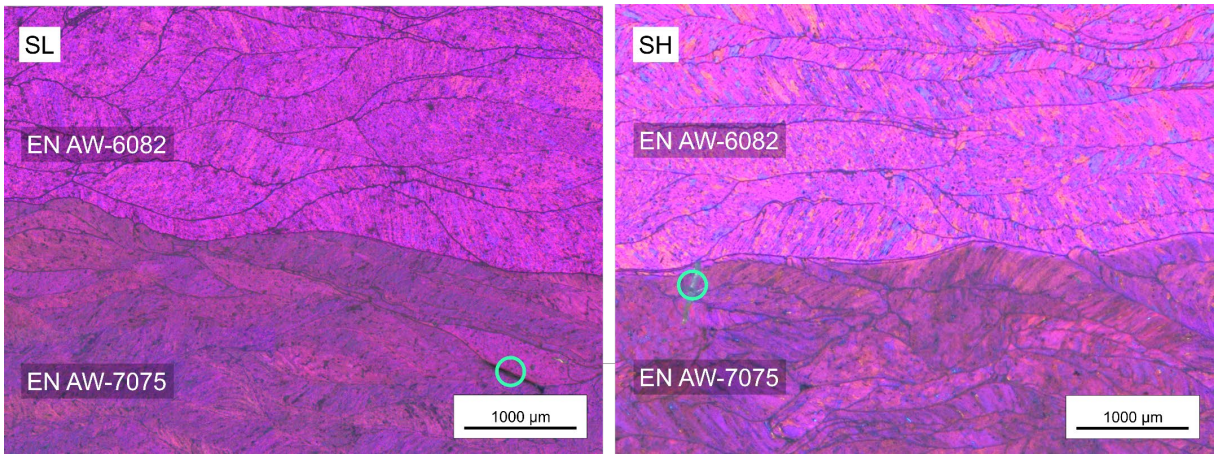

Fig. 5. Micrographs of the etched microstructure of the variants SL and SH in sintered condition. Defects are encircled in green.

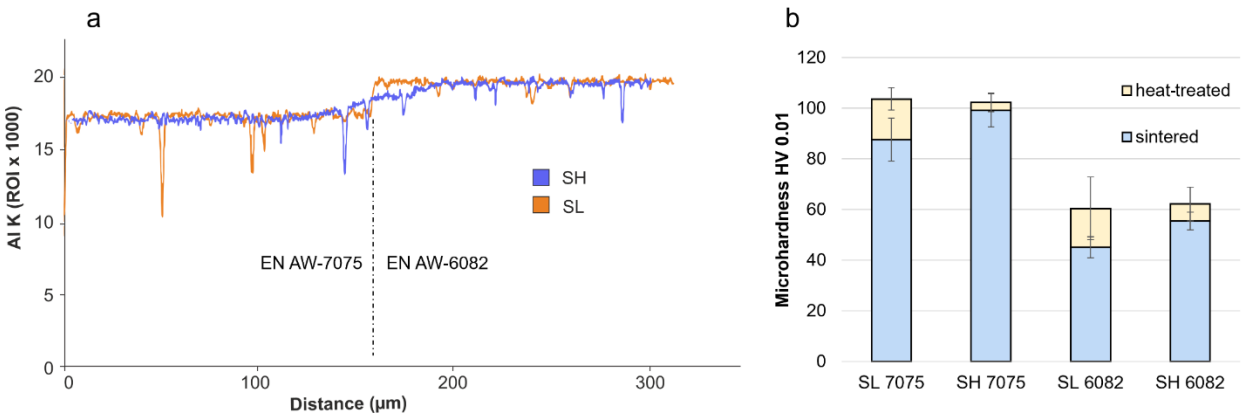

Fig. 6. Results of the EDX line scans (a) and the microhardness measurements (b) on the SL and SH variants.

After impact extrusion, the sintered microstructure is re-orientated in the direction of extrusion. Chips and chip boundary layers are stretched and elongated in the same direction (Fig. 7). This leads to the optical pronunciation of defects perpendicular to material extrusion, which were higher in number for the RL and SL variants than for RH and SH.

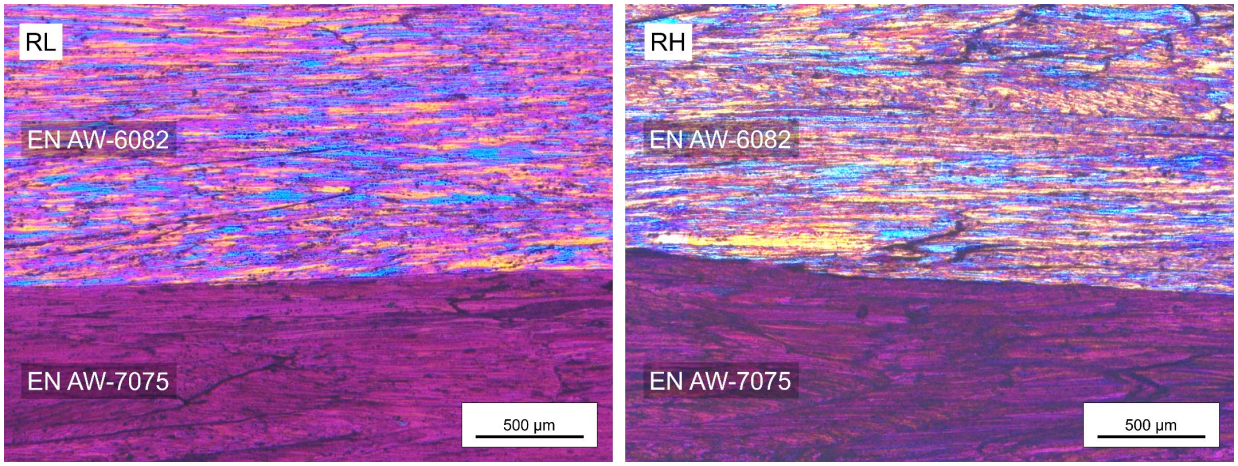

Fig. 7. Micrographs of the alloy interface of the radial variants RL and RH after extrusion.

After solution annealing and short cold aging, this deformed structure is recrystallized throughout the specimens. Fig. 8 shows metallographic images of the SH variant after the heat-treatment. While both alloys show coarse grains and few distinct chip boundaries, the material's orientation is still obvious in the EN AW-6082 and near the edge of the extruded shaft in the EN AW-7075 material. Furthermore, the interface shows a broad gradient in the etching/coloring, indicating growth of the diffusion zone. The results of the microhardness measurements in this heat-treated condition are given in Figure 6b. For both alloys, there is a significant increase in hardness over their respective low temperature variant in as-sintered condition. Compared to the values obtained from the SH variant, the hardness increase is smaller with only 4 HV 0.01 in case of EN AW-7075 and 7 HV in case of EN AW-6082 material.

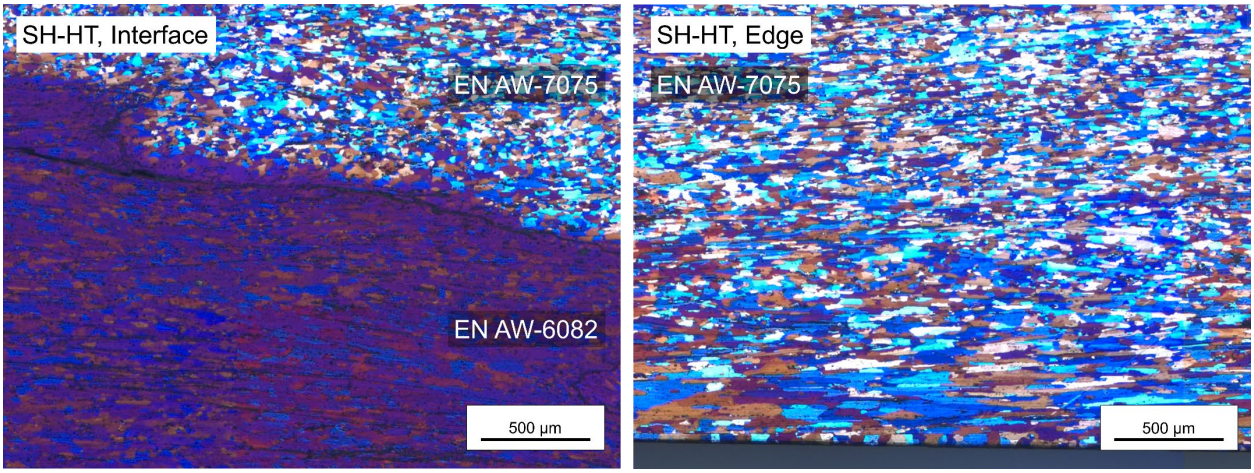

Fig. 8. Micrographs of the alloy interface of the edge of the part of the SH variant after extrusion and heat-treatment.

Discussion

The results indicate a significant influence of the sintering temperature on the diffusion processes across chip boundaries as well as on the microstructure within the individual aluminum chips. In previous work, tensile specimens were produced using the identical FAST process at 400°C for 5 min to recycle EN AW-6082 aluminum chips. After extrusion and T6 heat-treatment, the resulting tensile strength was comparable to the reference material in T6 condition at 379.8 MPa ultimate tensile strength and 354.7 MPa yield strength [22]. This indicates, that the presence of visible boundary layers between the chips may be tolerable for quasistatic properties. However, raising the sintering temperature to 500°C seems to activate diffusion mechanisms, which are not active or significantly reduced at 400°C. Due to the hybrid nature of the investigated specimens, this change could be observed in the material's response to etching and the EDX scans. Furthermore, recrystallization across the chip boundaries becomes more prevalent with higher temperature, effectively disrupting and dissolving the oxide layers. All defects, that were observed occurred in between chips. Hence, it may be assumed, that sintering at higher temperatures leads to increased formability and fatigue properties, because of fewer and smaller defects in the material.

The bond quality between the chips at the interface gains importance when creating hybrid parts form different alloys. These have different elastic and plastic material properties, which result in increased stresses on the interface during forming. This can be seen in Fig. 3 and 4 and is a challenge for all hybrid forming operations [26]. In the presented recycling process, defects were not reduced during cold impact extrusion, but deformed and elongated. Therefore, the FAST process needs to densify and consolidate the chips to a degree, which does not depend on further improvements through cold forming with low to medium plastic strains. Solution annealing after cold forming leads to complete recrystallization of the deformed microstructure after extrusion. The forming process still affects grain size and shape on the edge of the part. It is unclear whether this is due to increased local plastic strain or due to temperature gradients during annealing. In any case, the microstructure is reset to a condition with hardness similar to the as-sintered state and with a coarser and more homogeneous grain structure.

Finally, the presented recycling process allowed the production of hybrid parts with the potentially harder EN AW-7075 and the softer EN AW-6082 in two different layouts. The CT images indicate a nearly ideal macroscopic distribution of both alloys. However, metallography shows some curvature and localized interference of individual chips. The presented layouts were developed with potential application under torsional loads, using EN AW-7075 in the load-bearing outer area.

Summary

In summary, hybrid parts were successfully produced from aluminum chips of EN AW-6082 and EN AW-7075 alloys with a nearly defect-free structure. The geometry and distribution of both alloys within the billet after FAST and the final part after extrusion show little variance. Combined with reduced defect concentration and increased inter-chip diffusion due to increased sintering temperatures, promising results could be achieved. Using the presented process, the production of hybrid components directly from scrap material is feasible and can potentially be used to either compensate for inferior starting material with higher quality chips or to maximize part performance under certain loading conditions. Both aspects will be subject of further research.

Acknowledgements

The results presented were obtained in the project “Mechanism-based characterization and evaluation of the performance of resistively sintered semi-finished products based on recycled aluminum chips”, project no. 454199925. The authors thank the German Research Foundation (Deutsche Forschungsgemeinschaft, DFG) for their financial support.

References

[1] T.J. Brown, N.E. Idoine, E.R. Raycraft, R.A. Shaw, S.F. Hobbs, P. Everett, E.A. Deady, T. Bide, World Mineral Production 2012-16, Keyworth, Nottingham., 2018.

[2] Information on https://international-aluminium.org/resource/iai-material-flow-model-2021-update/

[3] R. Zhao, C. Nowicki, L. Gosselin, C. Duchesne, Energy and exergy inventory in aluminum smelter from a thermal integration point-of-view, Int. J. Energy Res. 40 (2016) 1321-1338. https://doi.org/10.1002/er.3508

[4] A. Gupta, B. Basu, Sustainable Primary Aluminium Production: Technology Status and Future Opportunities, Trans. Indian. Inst. Met. 72 (2019) 2135-2150. https://doi.org/10.1007/s12666-019-01699-9

[5] T.G. Gutowski, S. Sahni, J.M. Allwood, M.F. Ashby, E. Worrell, The energy required to produce materials: constraints on energy-intensity improvements, parameters of demand, Philos. Trans. A, Math. phys. eng. sci. 371 (2013) 20120003. https://doi.org/10.1098/rsta.2012.0003

[6] D. Brough, H. Jouhara, The aluminium industry: A review on state-of-the-art technologies, environmental impacts and possibilities for waste heat recovery, Int. J. Thermofluid. 1-2 (2020) 100007. https://doi.org/10.1016/j.ijft.2019.100007

[7] Information on https://www.umweltbundesamt.de/sites/default/files/medien/3521/dokumente/factsheet-aluminium_fi_barrierefrei.pdf

[8] Y. Xiao, M. Reuter, Recycling of distributed aluminium turning scrap, Miner. Eng. 15 (2002) 963-970. https://doi.org/10.1016/S0892-6875(02)00137-1

[9] M. Stern, U.S. Patent 2391,752 (1945).

[10] J. Gronostajski, A. Matuszak, The recycling of metals by plastic deformation: an example of recycling of aluminium and its alloys chips, J. Mater. Process. Technol. 92-93 (1999) 35-41. https://doi.org/10.1016/S0924-0136(99)00166-1

[11] J. Gronostajski, H. Marciniak, A. Matuszak, New methods of aluminium and aluminium-alloy chips recycling, J. Mater. Process. Technol. 106 (2000) 34-39. https://doi.org/10.1016/S0924-0136(00)00634-8

[12] J.Z. Gronostajski, J.W. Kaczmar, H. Marciniak, A. Matuszak, Direct recycling of aluminium chips into extruded products, J. Mater. Process. Technol. 64 (1997) 149-156. https://doi.org/10.1016/S0924-0136(96)02563-0

[13] V. Güley, A. Güzel, A. Jäger, N. Ben Khalifa, A.E. Tekkaya, W.Z. Misiolek, Effect of die design on the welding quality during solid state recycling of AA6060 chips by hot extrusion, Mater. Sci. Eng. A 574 (2013) 163-175. https://doi.org/10.1016/j.msea.2013.03.010

[14] M. Haase, A.E. Tekkaya, Cold extrusion of hot extruded aluminum chips, J. Mater. Process. Technol. 217 (2015) 356-367. https://doi.org/10.1016/j.jmatprotec.2014.11.028.
[15] M.I. Abd El Aal, M.A. Taha, A.I. Selmy, A.M. El-Gohry, H.S. Kim, Solid state recycling of aluminium AA6061 alloy chips by hot extrusion, Mater. Res. Express 6 (2019) 36525. https://doi.org/10.1088/2053-1591/aaf6e7
[16] B. Lela, J. Krolo, S. Jozić, Mathematical modeling of solid-state recycling of aluminum chips, Int. J. Adv. Manuf. Technol. 87 (2016) 1125-1133. https://doi.org/10.1007/s00170-016-8569-5
[17] N. Bay, Mechanisms Producing Metallic Bonds in Cold Welding, Weld. J. (1983) 137-142.
[18] D.R. Cooper, J.M. Allwood, The influence of deformation conditions in solid-state aluminium welding processes on the resulting weld strength, J. Mater. Process. Technol. 214 (2014) 2576-2592. https://doi.org/10.1016/j.jmatprotec.2014.04.018
[19] M. Haase, N. Ben Khalifa, A.E. Tekkaya, W.Z. Misiolek, Improving mechanical properties of chip-based aluminum extrudates by integrated extrusion and equal channel angular pressing (iECAP), Mater. Sci. Eng. A 539 (2012) 194-204. https://doi.org/10.1016/j.msea.2012.01.081
[20] J.R. Cui, W. Guo, H.J. Roven, Q.D. Wang, Y.J. Chen, T. Peng, Recycling of Aluminum Scrap by Severe Plastic Deformation.
[21] D. Paraskevas, K. Vanmeensel, J. Vleugels, W. Dewulf, Y. Deng, J.R. Duflou, Spark Plasma Sintering As a Solid-State Recycling Technique: The Case of Aluminum Alloy Scrap Consolidation, Mater. 7 (2014) 5664-5687. https://doi.org/10.3390/ma7085664
[22] A. Koch, M. Bonhage, M. Teschke, L. Luecker, B.-A. Behrens, F. Walther, Electrical resistance-based fatigue assessment and capability prediction of extrudates from recycled field-assisted sintered EN AW-6082 aluminium chips, Mater. Charact. 169 (2020) 110644. https://doi.org/10.1016/j.matchar.2020.110644
[23] C.N. Cislo, B. Kronthaler, B. Buchmayr, C. Weiß, Solid State Recycling of Aluminum Alloy Chips via Pulsed Electric Current Sintering, JMMP 4 (2020) 23. https://doi.org/10.3390/jmmp4010023
[24] R.H.R. Castro, K. van Benthem, Sintering: Mechanisms of convention nanodensification and field assisted processes, Springer, Berlin, New York, 2013.
[25] J. Fogagnolo, E. Ruiz-Navas, M. Simón, M. Martinez, Recycling of aluminium alloy and aluminium matrix composite chips by pressing and hot extrusion, J. Mater. Process. Technol. 143-144 (2003) 792-795. https://doi.org/10.1016/S0924-0136(03)00380-7
[26] B.A. Behrens, M. Bonhage, D. Bohr, D. Duran, Simulation Assisted Process Development for Tailored Forming, MSF 949 (2019) 101-111. https://doi.org/10.4028/www.scientific.net/MSF.949.101